South America Drought as a Precursor to Tropical Pacific Sea Surface Temperature Cooling

Wei Lou[1], Cheng Sun[*1], Fred Kucharski[2], Jianping Li[3,4], Jin-Yi Yu[5], Ruiqiang Ding[6], Antonietta Capotondi[7,8]

1 State Key Laboratory of Remote Sensing and Digital Earth, Faculty of Geographical Science, Beijing Normal University, Beijing 100875, China

2 Abdus Salam International Centre for Theoretical Physics, Trieste, Italy

3 Frontiers Science Center for Deep Ocean Multispheres and Earth System/Key Laboratory of Physical Oceanography/ Academy of the Future Ocean, Ocean University of China, Qingdao 266100, China

4 Laoshan Laboratory, Qingdao 266237, China

5 Department of Earth System Science, University of California, Irvine, CA, USA

6 State Key Laboratory of Earth Surface Processes and Hazards Risk Governance, Faculty of Geographical Science, Beijing Normal University, Beijing 100875, China

7 Cooperative Institute for Research in Environmental Sciences, University of Colorado, Boulder, CO, USA

8 Physical Sciences Laboratory, NOAA, Boulder, CO, USA.

*Corresponding author: Cheng Sun, scheng@bnu.edu.cn

ABSTRACT: South America has experienced notable drought conditions over recent decades. Concurrently, the adjacent tropical eastern Pacific has exhibited cooling anomalies in sea surface temperature (SST). Here, through observational analyses and climate model simulations, we reveal that terrestrial drought in central South America (CSA) acts as an emerging precursor to SST cooling in the tropical central-eastern Pacific (TCEP). Our statistical analysis identifies a robust lagged relationship whereby anomalous winter (December–February) TCEP SST cooling systematically follows reduced spring (March–May) CSA soil moisture. Employing diagnostic analyses of atmospheric and oceanic processes together with a hierarchy of climate models—including soil moisture sensitivity experiments, linear baroclinic model simulations,

Early Online Release: This preliminary version has been accepted for publication in *Journal of Climate*, may be fully cited, and has been assigned DOI 10.1175/JCLI-D-25-0407.1. The final typeset copyedited article will replace the EOR at the above DOI when it is published.

and fully coupled Earth system model experiments—we demonstrate a coherent mechanistic pathway in which reduced soil moisture in CSA triggers a subtropical-to-equatorial meridional precipitation dipole that disrupts Pacific zonal circulation, strengthen easterly trade winds, activates ocean–atmosphere feedbacks, and ultimately lead to cooling of TCEP SST in the subsequent winter. Our findings demonstrate a novel ocean-land-atmosphere coupling pathway modulating tropical Pacific variability, with significant implications for enhancing understanding of ocean-land-atmosphere interactions.

Key Words: Tropical Pacific SST cooling; South America terrestrial drought; Ocean-land-atmosphere coupling

1 Introduction

The tropical central-eastern Pacific (TCEP) sea surface temperature (SST) plays a crucial role in both regional and global climate system (Wang and Fiedler 2006), modulating tropical circulation and propagating global climate teleconnections (Liu and Sun 2023). The El Niño-Southern Oscillation (ENSO), the dominant mode of interannual climate variability, centers its core dynamics in the TCEP, where SST gradients drive coupled ocean-atmosphere feedbacks. (McPhaden et al. 2006). Decadal TCEP SST variability exerts substantial control over ENSO dynamics, modulating its amplitude, phase transitions, and decay phases (McPhaden et al. 2011), notably during triple-dip La Niña events linked to Pacific mean-state shifts (Li et al. 2023; Wang et al. 2023). Understanding the physical mechanisms underlying TCEP SST variability is therefore important for improving our understanding of ENSO dynamics and variability, and may provide useful insights into its predictability and future climate projections.

Satellite observations reveal SST anomalies characterized by cooling in the TCEP (Capotondi and Qiu 2023; Capotondi et al. 2023; England et al. 2014; Kosaka and Xie 2013). Existing research attributes this to both external forcing and internal variability (Chung et al. 2024; Latif et al. 2023). Within the Pacific, weakened nonlinear ENSO amplitude modulates the eastern Pacific mean state, contributing to cooling anomalies via mean-state rectification (Kohyama et al. 2017). Beyond the basin, Southern Ocean cooling via cloud-amplified global teleconnections (Kang et al. 2023) and tropical inter-basin interactions strengthen trade winds, driving tropical Pacific SST cooling (Luo et al. 2012; McGregor et al. 2014). Aerosols can also

Accepted for publication in *Journal of Climate.* DOI 10.1175/JCLI-D-25-0407.1.

induce rapid Hadley cell adjustment and Southeast Pacific cloud feedbacks, contributing to tropical Pacific SST cooling (Hwang et al. 2024). Despite advances in ocean-atmosphere coupling understanding, debate persists over primary mechanisms, as historical forcing experiments rarely reproduce observed SST cooling patterns (Seager et al. 2022). Recent idealized experiments highlight terrestrial ecosystem changes-particularly tropical deforestation-as modulators of ENSO dynamics through regional precipitation alterations (Lee et al. 2023; Wei et al. 2024). However, specific mechanisms linking land-ocean-atmosphere interactions to tropical Pacific climate variability remain poorly understood.

South America, located adjacent to the tropical Pacific, has experienced significant increase in the frequency and severity of droughts in recent years (Feron et al. 2024). These droughts, particularly in central South America (CSA), have intensified and exerted profound impacts on local ecosystems, agriculture, and water resources (Geirinhas et al. 2021; Lou et al. 2026). Multiple factors contribute to drought development in CSA. Elevated greenhouse gas concentrations can disrupt regional hydrothermal circulation and monsoon systems, leading to reduced precipitation (Brito et al. 2023; Chiang et al. 2021), while large-scale deforestation can further exacerbate land aridity by altering land–atmosphere interactions and reducing regional moisture recycling (Staal et al. 2020; Xu et al. 2022). Tropical SST variability also plays a crucial role in modulating the hydroclimate of this region. ENSO variability has been demonstrated to strongly affect drought conditions in CSA, and anomalous SSTs in the North Atlantic may further intensify drought severity by altering regional atmospheric subsidence (Cai et al. 2020; Espinoza et al. 2024; Zeng et al. 2008).

Soil moisture (SM) serves as a key indicator for monitoring drought in CSA region, modulating land-atmosphere interactions by regulating surface evapotranspiration (Jiang and Wang 2024; Spennemann and Saulo 2015). In this region, SM exhibits pronounced interannual variability and is markedly reduced during recent extreme drought events. During drought episodes, the thermal memory of SM can amplify these feedbacks, prolonging drought duration and intensifying its severity (Geirinhas et al. 2023; Mondal et al. 2024). Through its influence on evaporation, hydrology, and circulation, SM–atmosphere interactions also affect regional precipitation, moisture transport, and the severity of drought–heat extremes (Chen and Dominguez 2024; Jiang and Wang 2024; Poveda and Mesa 1997). While the influence of ocean

Accepted for publication in *Journal of Climate*. DOI 10.1175/JCLI-D-25-0407.1.

variability on continental hydroclimate is well established, the role of land surface processes in modulating ocean climate variability remains less explored. Increasing evidence suggests the existence of two-way land–ocean coupling. For example, intensified Amazon droughts have been shown to amplify SST warming in the tropical North Atlantic through changes in large-scale atmospheric circulation and air–sea heat exchange (Lou et al. 2024b). However, whether terrestrial droughts in CSA can influence climate variability in the tropical Pacific remains unclear.

Recent extreme hydrological drought crisis in South America have drawn significant scientific interest. These prolonged and widespread droughts may disrupt tropical atmospheric circulation, thereby influencing tropical ocean dynamics through complex land-atmosphere-ocean interactions. From a new perspective focusing on land-to-ocean linkages, this study shows dry South America SM may as a precursor of TCEP SST cooling, revealing how land surface processes influence ocean dynamics via atmospheric teleconnections and ocean-atmosphere coupling processes.

2 Data and methods

2.1 Data and definitions of climate indices

In this study, the SST data is obtained from Extended Reconstructed SST version 5 (available at https://psl.noaa.gov/data/gridded/data.noaa.ersst.v5.html)(Huang et al. 2017). The subsurface ocean temperature data is derived from the Met Office Hadley Centre observation datasets EN4.2.1 (available at https://climatedataguide.ucar.edu/climate-data/en4-subsurface-temperature-and-salinity-global-oceans)(Good et al. 2013). The top layer of SM for global terrestrial surfaces and the atmospheric data for sea level pressure, vertical velocity, surface winds are derived from the ECMWF reanalysis, ERA5(Hersbach et al. 2020). The precipitation data is from CPC Merged Analysis of Precipitation (CMAP)(Xie and Arkin 1997). We also use the SST data from Met Office Hadley Center(Rayner et al. 2003), Kaplan(Kaplan et al. 1998), Centennial in situ Observation-Based Estimates(COBE)(Ishii et al. 2005) and SM dataset from Terra Climate(Abatzoglou et al. 2018) for complementary validation. To describe the drought, we also use the Standardized Precipitation Index (SPI) as a supplement to SM. All data are monthly and available for the period 1991-2022. The raw datasets are regridded to the T42 grid

Accepted for publication in *Journal of Climate*. DOI 10.1175/JCLI-D-25-0407.1.

to facilitate a comparison among different data sources.

In this study, the TCEP SST index is defined as the averaged SST in the region of (10°S-10°N,170°W-110°W) in the tropical Pacific. The CSA SM index is defined as the averaged SM in the region of (20°S–10°S,65°W–45°W) in the South America. The equatorial central-western Pacific (ECWP) zonal wind index is defined as the averaged zonal wind in the region of (5°S–5°N, 180°W–160°W) in the tropical Pacific. The South America precipitation dipole index is defined as the difference between averaged precipitation anomalies over equatorial South America and adjacent tropical Atlantic (ESA&TA, 0°–10°N, 68°W–50°W) and those over CSA (20°S–10°S,65°W–45°W). The Niño3.4 index is defined as the average of SST anomalies over the Niño3.4 region (5°S–5°N, 170°W–120°W). This study adopts the Northern Hemisphere seasonal division standard: winter is defined as December-January-February (DJF) and spring is defined as March-April-May (MAM). We specifically focus on the relationship between spring CSA SM and the subsequent winter TCEP SST, as winter exhibits the strongest cooling trend and spring SM shows the most robust lead-lag coupling with winter SST (detailed in Section 3.1).

2.2 Methods and Model experiment

Linear baroclinic model

This study employs the Linear Baroclinic Model (LBM) to explore steady atmospheric responses to simultaneous idealized diabatic heating and cooling representing the north-south precipitation dipole's diabatic heating pattern. The LBM is based on atmospheric primitive equations linearized around a mean state and can simulate the steady linear response to a prescribed forcing, and it has been widely used in simulating atmospheric responses to specified diabatic heating. The model has a horizontal resolution of T21 and 20 sigma levels. Rayleigh friction and Newtonian damping employ an e-folding time of one day for the top two layers and the bottom three layers, 5 and 15 days for the fourth and fifth layers, and 30 days for the other model layers (Watanabe and Jin 2003). The vertical structure of the heating is characterized by a gamma distribution function, with maximum amplitude in the mid-troposphere (Deng and Dai 2024). We utilize the climatological spring (March-April-May) mean state for the time period 1991–2022 from the NCEP/NCAR Reanalysis as the basic state. The model is integrated

Accepted for publication in *Journal of Climate*. DOI 10.1175/JCLI-D-25-0407.1.

for 30 days with the fixed diabatic heating anomaly, and the results averaged for the last 10 days are analyzed, as the atmosphere can reach its steady state in 15 days(Watanabe and Jin 2003). In this study, the large-scale precipitation-related source heating is imposed over the ESA&TA region (0°–10°N, 68°W–50°W) with a peak of 5 K/day at 500 hPa to simulate the effect of large-scale precipitation-like heating anomaly (Appendix Fig.A1a). The diabatic cooling source is imposed over the CSA region (20°S–10°S, 65°W–45°W) with a peak magnitude of -5 K/day at 500 hPa to simulate diabatic cooling associated with precipitation reduction induced by SM deficits (Appendix Fig. A1b).

A sensitivity experiment examining the tropical atmospheric response to the reduction of soil moisture in South America

To assess the atmospheric response to SM depletion over South America, we utilize the ICTP General Circulation Model (ICTPGCM) with its SPEEDY atmospheric component (Kucharski et al. 2006). SPEEDY is a spectral atmospheric general circulation model (AGCM) featuring eight vertical layers and T30 horizontal resolution, incorporating key physical parameterizations—convection, condensation, cloud processes, radiative transfer, and vertical mixing. The land surface model is interactively coupled, permitting the exchange of energy, water, and momentum with the atmosphere, while exhibiting a capacity for simulating climate and surface physical processes (Gore et al. 2020). This model has demonstrated robust performance in numerous studies examining the complex feedbacks between land surface conditions, atmospheric circulation patterns, and oceanic forcing (Kucharski et al. 2013a; Kucharski et al. 2013b; Lou et al. 2023; Lou et al. 2024b; Schumacher et al. 2022).

The experimental protocol consists of two experiments—a control run (SM_Ctrl) and a sensitivity experiment (SM_Deficit)—each configured as an ensemble of five members. This ensemble size follows previous studies and is sufficient to robustly extract the forced signal (Molteni et al. 2024). Each member is initialized from different atmospheric initial conditions. SM_Ctrl demonstrates a strong capacity to capture observed key regional circulation features, making it a robust baseline for comparison (Fig.S1). Both experiments prescribe monthly climatological SSTs derived from ERSSTv5 (Fig.S2a). In SM_Ctrl, SM (both top soil layer and root zone) follows its monthly climatology derived from ERA5 (Fig.S2b). In SM_Deficit, SM

Accepted for publication in *Journal of Climate.* DOI 10.1175/JCLI-D-25-0407.1.

is prescribed as the climatological mean superimposed with an anomaly term within the CSA domain (20°S–10°S, 65°W–45°W) during the spring (March–May, MAM) season. This anomaly is defined as the product of the observed spring SM linear trend value during 1991–2022 and an amplification factor of five. The fivefold amplification is used solely to enhance signal detectability given the finite ensemble size and integration length. Both ensembles are integrated for 50 years, with the initial 30 years discarded as spin-up. The final spring (MAM) atmospheric response is quantified as the difference between SM_Deficit and SM_Ctrl ensemble means, normalized by the scaling factor of five. This framework isolates the impact of South America SM reduction on tropical atmospheric dynamics. The experimental design in this study is similar to that of Lou et al. (2024), which involves a sensitivity modeling experiment on SM over the Amazon region, focusing on the impact of drying SM anomalies on the Atlantic Ocean (Lou et al. 2024b).

Pseudo-ensemble sampling

The main goal of this approach is to search for 30-year-long periods within simulations that exhibits obvious trends. This pseudo-ensemble is used as an analog of the given model's internal climate physics in the absence of anthropogenic forcing. We use a 1200-year CESM2 preindustrial control (PI-Control) simulation, a fully coupled experiment designed to assess the contribution of internal climate variability to recent changes in atmospheric circulation, absent any anthropogenic forcing. Preliminary evaluation confirms that this model faithfully reproduces observed CSA SM -TCEP SST relationship (Fig.S3). We calculate the 30-year sliding linear trend of the simulation data, resulting in a set of 1170 samples. To ensure stability and representativeness by eliminating initial drifts capturing long-term trend more effectively, and aligning with established methodologies in climate research, we begin our analysis from the 500th sample, resulting in more reliable and scientifically valid results. We identify a subset of samples representing CSA SM anomalies by selecting those with trends values greater than one standard deviation, ensuring statistical significance, reducing noise, and capturing extreme events. We then perform composite analyses of SST, zonal wind, and velocity potential trends for these selected samples.

Statistical analysis

To characterize the coupled variability between tropical Pacific SST and South America

Accepted for publication in *Journal of Climate*. DOI 10.1175/JCLI-D-25-0407.1.

SM, we employ the Singular Value Decomposition (SVD) method (Bretherton et al. 1992). Specifically, we perform SVD on the cross-covariance matrix derived from winter (December−February, D0JF1, where "0" refers to the current year and "1" refers to the subsequent year) tropical Pacific SST anomalies and spring (March−May, MAM0) South America SM anomalies. The leading SVD mode captures the dominant coupled spatial patterns and their temporal evolution.

To rigorously assess the statistical significance of winter TCEP SST differences in association with anomalously dry spring CSA SM, we apply the bootstrap resampling method (Austin and Tu 2004). Spring CSA SM anomalies are divided into wet (anomaly > 0) and dry (anomaly < 0) categories. For each group, the corresponding winter TCEP SST anomaly indices are resampled with replacement over 10,000 times, producing empirical distributions of the mean values. The standard deviation of each bootstrap mean distribution is calculated. The difference between the mean TCEP SST anomalies for dry and wet conditions is considered statistically significant at the 95% confidence level if it exceeds twice the sum of the standard deviations from both bootstrap distributions.

We also employ a series of statistical techniques to analyze the data, including regression, correlation, partial correlation, partial regression and composite analyses. Linear trends in time series and datasets are determined using the Theil–Sen trend estimation method (Sen 1968). To assess potential changes in trends, we implement a statistical t-test to compare the slopes of two sub-periods partitioned at the identified turning point, following the methodology described by Zuo (Lou et al. 2024a; Zuo et al. 2020).

For significance testing of correlations between autocorrelated time series, we apply a two-sided Student's t-test (Lou et al. 2023; Lou et al. 2024b). The effective degrees of freedom N^{eff} are calculated according to the following expression [Eq. 2] (Li et al. 2013):

$$\frac{1}{N^{eff}} \approx \frac{1}{N} + \frac{2}{N}\sum_{j=1}^{N}\frac{N-j}{N}\rho_{XX}(j)\rho_{YY}(j) \tag{2}$$

where N is the total sample size, $\rho_{XX}(j)$ and $\rho_{YY}(j)$ denote the autocorrelation coefficients of series X and Y at lag j, respectively.

3 Results

3.1 The cross-seasonal connection between CSA SM and TCEP SST

Accepted for publication in *Journal of Climate*. DOI 10.1175/JCLI-D-25-0407.1.

Recent research indicates that cool SST anomalies has prevailed in the tropical Pacific since the 1990s (Capotondi and Qiu 2023; Capotondi et al. 2023; England et al. 2014). Consistent with these prior findings, our analysis shows wintertime SST changes in tropical eastern Pacific around the 1990s (Fig. 1 and Fig.S4), with winter exhibiting the strongest cooling among all seasons (Fig. S5a). This feature in SST is robustly captured across multiple datasets. Concurrent with this oceanic transformation, South America has experienced frequent terrestrial droughts in recent years, driven primarily by intensified deforestation and anthropogenic disturbances (Zalles et al. 2021). Both the SPI and terrestrial SM exhibit statistically significant declines across the continent (Fig. S6), with the most pronounced reductions concentrated over CSA region. To investigate whether variations in preceding South America SM could influence tropical Pacific SST variability, we analyze the lead-lag relationship between CSA SM and winter TCEP SST. The analysis reveals a prominent interannual coupling, whereby spring CSA SM anomalies clearly lead winter TCEP SST variations (Fig. S5b). This indicates that spring CSA SM anomalies may emerge as a precursor signal for subsequent winter TCEP SST change. Thus, we focus on the spring CSA SM–winter TCEP SST linkage to elucidate the underlying physical mechanisms.

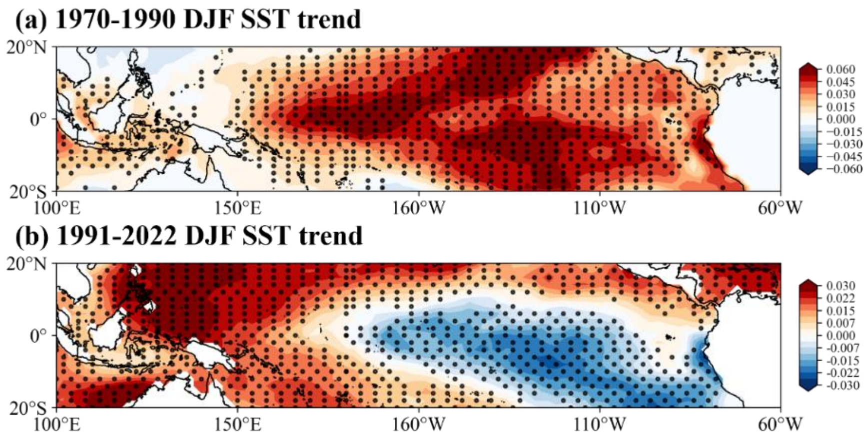

Fig. 1. **(a)** Winter SST linear trends (°C per year) during 1970-1990. **(b)** Same as **(a)** but for 1991-2022. Stippled regions indicate where all four SST datasets (ERSSTv5, HadISST, Kaplan and COBE) agree on the sign of the slope.

To explore the potential link between drought conditions in South America and tropical Pacific SST variability, we perform SVD analysis using spring SM and winter SST fields. The leading left singular vector, which characterizes the winter tropical Pacific SST pattern, exhibits

Accepted for publication in *Journal of Climate*. DOI 10.1175/JCLI-D-25-0407.1.

predominantly negative loadings, with the maximum magnitude centered over the TCEP region. Correspondingly, the leading right singular vector, representing spring SM variability across South America, shows negative anomalies primarily concentrated in the CSA region. To assess the robustness of these patterns, we repeat the analysis using detrended SST and SM datasets, and the resulting spatial structures remained largely consistent. As illustrated in Figure 2, a significant spatiotemporal co-variation pattern is identified between winter (D0JF1) TCEP SST and spring (MAM0) CSA SM, with a correlation coefficient of 0.66 for expansion coefficients derived from the SVD analysis ($p<0.05$). These results are further corroborated using additional SM dataset (Fig.S7).

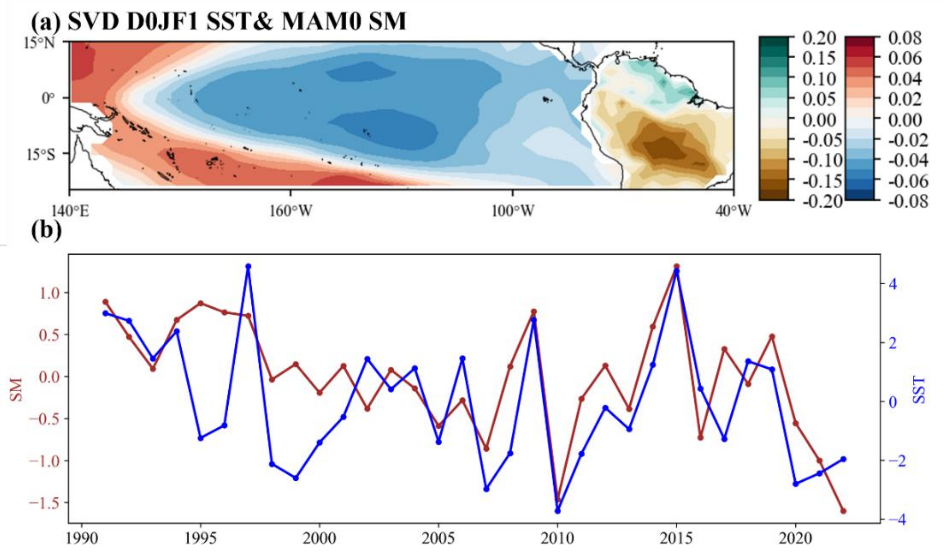

Fig. 2. (a) The spatial pattern of SVD first mode for the Tropical Pacific SST (25°S–15°N,140°E–70°W) in winter and the South America SM (30°S–10°N, 80°W–30°W) in spring from 1991 to 2022. **(b)** The corresponding normalized expansion coefficients. All datasets underwent linear detrending and standardization prior to analysis.

Based on the SVD results, we define two key indices the TCEP SST index and the CSA SM index, to quantitatively represent the regional climate variables outlined by the boxes in Fig. 3a. A comprehensive lead-lag correlation analysis is conducted to examine the temporal relationship between these two indices, revealing a statistically significant positive interannual correlation between spring CSA SM and the subsequent winter TCEP SST (Fig. 3a). The time series of both variables display coherent interannual fluctuations (Fig. 3b), with a correlation coefficient of $r = 0.58$ ($p < 0.05$) for the 1991–2022 period. This relationship remains robust after linear detrending ($r = 0.58$, $p < 0.05$, Fig.S8). Liang-Kleeman information flow analysis

Accepted for publication in *Journal of Climate*. DOI 10.1175/JCLI-D-25-0407.1.

identifies a statistically significant information flow from springtime CSA SM to the subsequent winter TCEP SST, suggesting that variations in CSA SM may serve as a potential precursor to TCEP SST anomalies (Fig.S9a, detailed methodological procedures are provided in the supplementary information). Notably, over the full 1950–2022 period, the correlation remains significant ($r = 0.28$, $p < 0.05$). The sliding correlation further shows that after the 1990s, the relationship becomes more stable and stronger (Fig.S10). Studies have shown that ERA5 benefits from a rapidly increasing volume of satellite observations assimilated into the reanalysis system after the 1990s (Hersbach et al. 2020; Muñoz-Sabater et al. 2021), which substantially improves the representation of atmospheric and land-surface variables, including SM. The enhanced post-1990 signal may therefore reflect both a physically robust linkage and improved reanalysis fidelity. Consequently, this study focuses on elucidating the physical mechanisms underlying CSA SM-TCEP SST linkage post-1990.

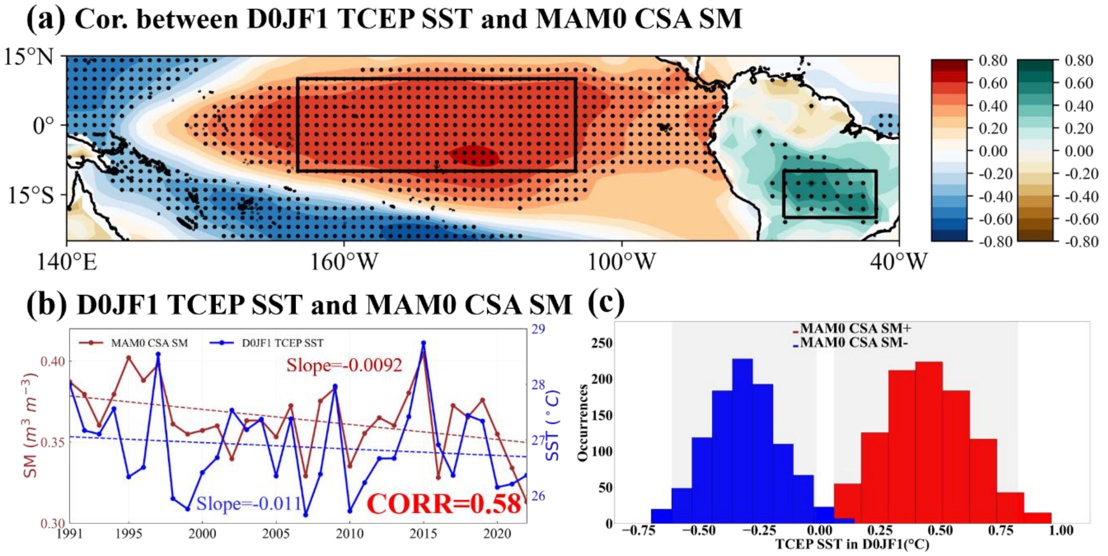

Fig. 3. The correlation map of the MAM0 CSA (black box in the figure, 20°S–10°S, 65°W–45°W) SM index with **(a)** D0JF1 SST (blue and red color in the figure). The correlation map of the D0JF1 TCEP (10°S–10°N, 170°W–110°W) SST index with **(a)** MAM0 SM (brown and green color in the figure). **(b)** The corresponding time series of D0JF1 TCEP SST index and MAM0 CSA SM index for the period 1991–2022. They are defined as the weighted average of SST within the region (10°S–10°N, 170°W–110°W) and the weighted average of SM within the region (20°S–10°S, 65°W–45°W), respectively. The dotted shading indicates the correlation is significant at the 95% confidence level. **(c)** The histogram of 10,000 realizations of the bootstrap method for the winter TCEP SST anomaly indices following the spring CSA SM anomaly. Vertical red and blue bars indicate the mean values of 10,000 inter-realizations for the winter TCEP SST index, respectively. Gray shaded regions indicate the respective doubled standard deviations (SDs; the 95% confidence interval based on the normal distribution) of the

Accepted for publication in *Journal of Climate*. DOI 10.1175/JCLI-D-25-0407.1.

10,000 values. If the gray shaded regions do not overlap each other, then the statistical significance is above the 95% confidence level.

It is well-documented in the existing literature that SST anomalies in other tropical ocean basins exert significant influences on the evolution of tropical Pacific SST patterns. For instance, the warming of the Northern Tropical Atlantic SST serve as a trigger for La Niña event in the following winter(Ham et al. 2013). Amplified warming in the tropical Indian Ocean also contributes to the formation of La Niña-like SST anomalies in the equatorial Pacific(Luo et al. 2012). To isolate the specific effect of CSA SM on TCEP SST, we conduct a partial correlation analysis. After controlling for these oceanic influences, the relationship between spring CSA SM and winter TCEP SST remains statistically robust (Fig.S11), further reinforcing the specificity of the linkage between these two variables. Moreover, the CSA SM–TCEP SST linkage remains robust ($r = 0.44$, $p < 0.05$) even after the linear signal of NTA SST is strictly removed. We use a bootstrap resampling approach to evaluate whether winter SST anomalies in the TCEP differ significantly following negative spring SM anomalies over the CSA (Fig. 3c). The resulting probability distribution under the null hypothesis indicates that such negative SM anomalies are typically followed by a statistically significant cooling of winter SST in the TCEP. Collectively, these multi-faceted statistical analyses converge to establish a robust and consistent connection between winter TCEP SST and spring CSA SM, warranting further investigation into the underlying linkage mechanisms.

3.2 The physical process associated with the influence of CSA SM on TCEP SST

Variations in atmospheric winds play a crucial role in modulating tropical Pacific SST variability (Capotondi and Qiu 2023). The observed strengthening of tropical trade winds over recent decades has been identified as a direct driver of equatorial Pacific cooling(England et al. 2014). Against this background, our study further investigates the impact of CSA SM on tropical Pacific surface winds and SST.

Lagged regressions of SST and low-level wind anomalies onto the CSA SM index in MAM are performed. To visualize the impacts associated with reduced CSA SM, the regression fields are multiplied by minus one. During boreal spring (the MAM season; Fig.4a), easterly anomalies initially develop over the ECWP. These anomalies gradually extend eastward

Accepted for publication in *Journal of Climate*. DOI 10.1175/JCLI-D-25-0407.1.

through summer and autumn (Fig.4b-c), ultimately leading to a pronounced cooling of SST in the TCEP SST by winter (Fig.4d). Throughout this process, correlations between spring ECWP zonal winds and TCEP SST remain highly significant across all lead–lag time scales (Fig. 5a and Fig. 5c), peaking at AMJ0 lag and indicating tight coupling between winds and SST. Spring CSA SM exhibits significant zero-lag correlation with ECWP zonal winds (MAM0, Fig. 5b), whereas its linkage with TCEP SST emerges at a one-month lag (AMJ0) and strengthens thereafter., suggesting that zonal wind anomalies precede SST anomalies. These temporal relationships demonstrate that zonal wind anomalies systematically precede SST anomalies, consistent with the canonical Bjerknes positive feedback mechanism. Thus, springtime CSA SM anomalies likely serve as an upstream precursor that modulates tropical western Pacific zonal winds, ultimately contributing the lagged evolution of TCEP circulation and SST.

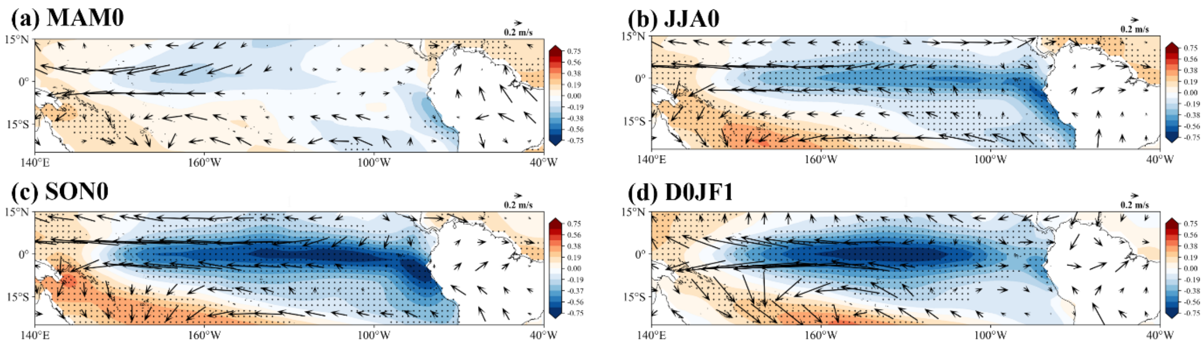

Fig. 4. (a) The regression map of the MAM0 CSA SM index with MAM0 850 hPa winds (units: m/s, vectors) and SST (units: °C, shading) for the period 1991–2022 (multiplied by −1). **(b), (c)** and **(d)** are same as **(a)**, but for JJA0, SON0 and D0JF1. The dotted shading indicates the regression is significant at the 95% confidence level.

Based on the results of the lead-lag correlation coefficients above, combined with the Liang−Kleeman information flow analysis method, the relationship between CSA SM and tropical Pacific zonal wind is further analyzed (Fig.S9b). The results reveal significant information flow from spring CSA SM to zonal wind anomalies over the ECWP. Furthermore, previous research has exactly pointed out that spring zonal winds play a pivotal role in ENSO development and tropical Pacific ocean variability(Cao et al. 2024; Capotondi et al. 2018), strongly supporting our research. More Importantly, the anomalous zonal wind response in the tropical Pacific to reduced CSA SM remains significant even after removing the influences of SST anomalies from Indian Ocean and Atlantic SST anomalies (Fig.S12) (Ham et al. 2013; Luo et al. 2012). The persistence and equatorward evolution of surface wind, latent heat flux, and

Accepted for publication in *Journal of Climate*. DOI 10.1175/JCLI-D-25-0407.1.

SST anomalies are typically associated with Wind-Evaporation-SST feedback over the tropical Pacific(Amaya et al. 2019; Huang et al. 2025), thereby leading to SST cooling in the ECWP. During summer, the surface wind fields associated with atmospheric circulation pattern characterized by deep convection exhibit easterly wind anomalies in the tropics, contributing to the persistence of SST anomalies(Huang et al. 2025; Vimont et al. 2003). The ECWP easterly flow effectively triggers a cooling of the eastern equatorial Pacific SST by shoaling the eastern equatorial thermocline(Bjerknes 1969). Specifically, intensified easterly winds drive surface warm water westward, causing equatorial upwelling. Through Ekman transport, cold water rises from the subsurface, resulting in a shallower thermocline and cooling SST in the eastern Pacific (Fig.4 and Fig.S13). The increased zonal SST gradient subsequently enhances easterly winds by promoting atmospheric convection above the warm pool and intensifying the zonal pressure gradient at sea level. With the cumulative effect of the positive air-sea feedback mechanism, this ultimately leads to the formation of a significant cool SST anomaly in the TCEP region during winter.

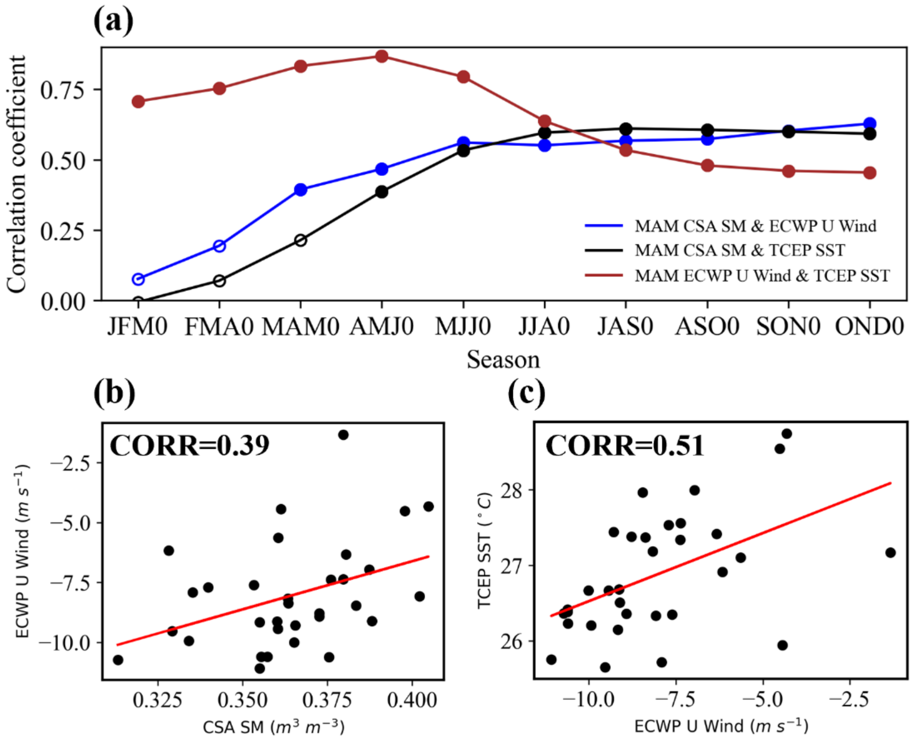

Fig. 5. (a) Lead–lag correlation between the spring CSA SM index and ECWP 850 hPa zonal wind index (blue), and TCEP SST (black), respectively. Lead–lag correlation between the spring ECWP 850 hPa zonal wind index and TCEP SST (red). Filled circles denote correlations

Accepted for publication in *Journal of Climate*. DOI 10.1175/JCLI-D-25-0407.1.

significant at the 90% level. **(b)** The scatter plot shows the relationship between spring CSA SM and spring ECWP 850 hPa zonal wind. **(c)** The scatter plot shows the relationship between spring ECWP 850 hPa zonal wind and winter TCEP SST. The red line represents the regression line of the scatterplot.

Then we analyze how declined SM in South America trigger easterly wind anomalies in the equatorial Pacific. Robust land–atmosphere interactions over South America sustain a substantial fraction of regional precipitation through evapotranspiration-driven feedback cycles (Eltahir and Bras 2010). These interactions enable SM anomalies to modulate local circulation and moisture transport via surface energy balance perturbations, with remote impacts transmitted through atmospheric teleconnections (Giles et al. 2022). Consequently, land–atmosphere feedback over the CSA likely plays a critical role in linking spring SM anomalies to winter TCEP SST variability. SM typically exhibits multi-month memory, sustaining wet or dry anomalies over extended periods (Seneviratne et al. 2004). Consistent with this, our analysis reveals strong seasonal persistence of spring CSA SM anomalies, with significant positive autocorrelations extending into summer (Fig.S14a-b). This persistence is maintained by coupled land-atmosphere feedbacks: spring CSA SM anomalies exhibit robust positive correlations with precipitation and evaporation (Fig. S14c-d), whereby reduced SM suppresses evaporation and low-level moisture convergence. The consequent precipitation deficit fails to replenish SM, thereby perpetuating the dry anomaly through a positive land–atmosphere feedback loop. Through this persistent dry forcing, spring CSA SM deficits establish prolonged surface boundary conditions that modulate regional precipitation patterns and large-scale atmospheric circulation. Consequently, the memory effect of dry CSA SM anomalies provides a critical physical mechanism linking land surface variability to delayed tropical Pacific SST responses.

Regression analysis of large-scale atmospheric circulation fields against the spring CSA SM index (Figs. 6a-b) reveals that SM deficits over the CSA significantly induce regional atmospheric dynamics anomaly. Specifically, the CSA SM deficits tend to reduce latent heat flux and boundary-layer moisture availability, thereby increasing the lower-tropospheric moist static stability. This enhanced atmospheric stability suppresses convection by reducing air parcel buoyancy and increasing convective inhibition (Seneviratne et al. 2010). As a result, pronounced local subsidence anomalies emerge in the mid-to-lower troposphere (Fig. 6a and

Accepted for publication in *Journal of Climate*. DOI 10.1175/JCLI-D-25-0407.1.

Fig.S15 a-b), accompanied by an increase in geopotential height and the development of anomalous southerly flow at low levels (Fig. S15c). These dynamical responses are further associated with enhanced regional moisture divergence (Fig.S15 d) and a marked decrease in specific humidity and column-integrated water vapor (Fig. S15 e), jointly contributing to the observed reduction in local precipitation (Fig. 6b). Moreover, owing to the persistence of SM anomalies, the associated circulation anomalies are maintained throughout the season (Fig. S16), exerting subsequent influence on the evolution of large-scale atmospheric circulation.

Based on combined spatial and lead-lag correlation analyses, we reveal that South America precipitation and SM exhibit a significant north-south dipole distribution pattern during spring (Fig.S17). This dipole structure suggests that when SM deficits occur in the CSA, it tends to induce compensatory precipitation changes in the ESA&TA. Acting as a critical link, this precipitation dipole bridges the CSA SM and TCEP SST (Fig.S18a-b). Specifically, the enhanced subsidence over the CSA region induces a compensating circulation, whereby intensified updrafts and low-level moisture convergence develop over ESA&TA, leading to increased precipitation in that area (Fig. 6b). The resultant low-level convergence and upper-level divergence over ESA&TA strengthen ascending motion, which propagates westward as anomalous zonal circulation—inducing compensating downdrafts over the central tropical Pacific (Figs. 6c-d). Regression of the precipitation dipole index onto velocity potential fields confirms this circulation response (Fig. S18c). Over the central tropical Pacific, descending air generate low-level anticyclonic anomalies, which in turn trigger easterly wind anomalies across the equatorial central-western Pacific (ECWP; Fig. 6e). These anomalous easterlies couple with the ocean via enhanced wind stress curl and Ekman pumping, shallowing the thermocline in the TCEP region and promoting upwelling of cold subsurface waters—ultimately driving SST cooling. Notably, the ESA&TA velocity potential exhibits a slight northward shift, which may be associated with enhanced divergence arising from suppressed convection over CSA.

Accepted for publication in *Journal of Climate.* DOI 10.1175/JCLI-D-25-0407.1.

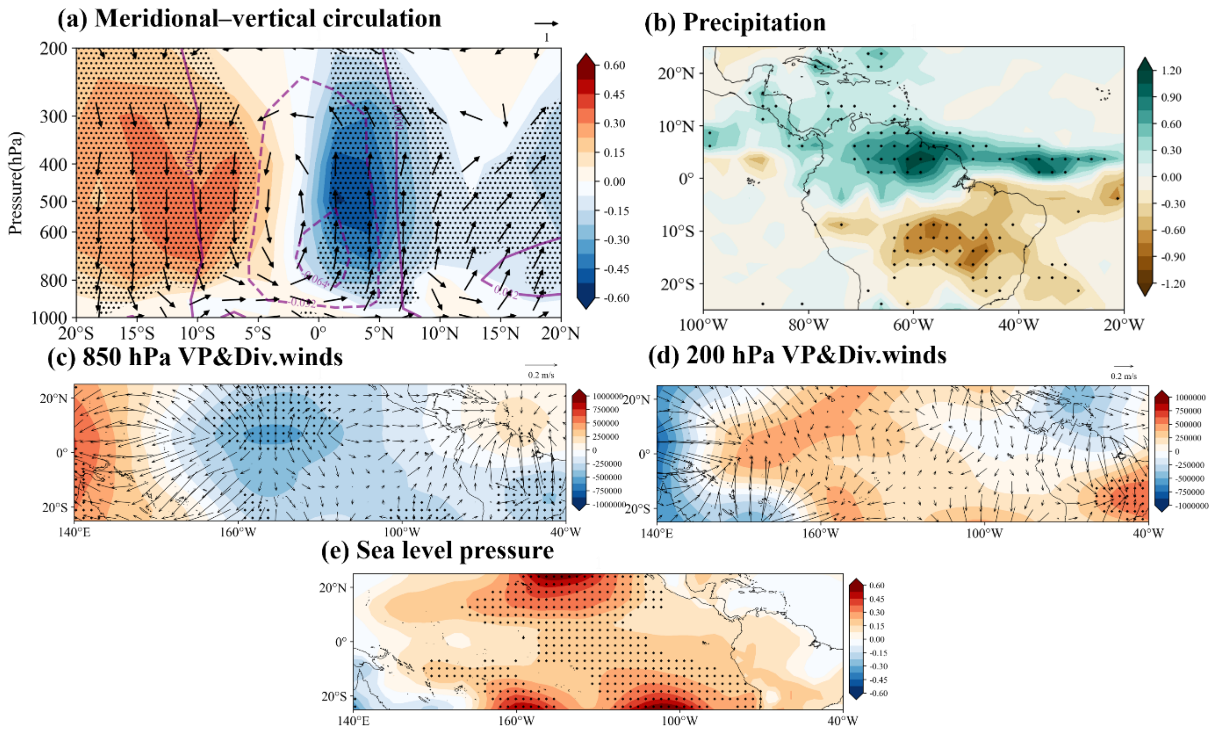

Fig. 6. Regression of the spring **(a)** meridional–vertical circulation anomalies averaged between 70°W–40°W (vectors) and vertical velocity anomalies (units: Pa/s, shading, contours represent spring climatology), **(b)** precipitation (units: mm/day, shading), **(c)** 850 hPa velocity potential (units: m^2/s, shading) and divergent wind (units: m/s, vectors), **(d)** 200 hPa velocity potential (units: m^2/s, shading) and divergent wind (units: m/s, vectors) and **(e)** sea level pressure (units: hPa, shading) with the MAM0 CSA SM index for the period 1991–2022 (multiplied by −1). The dotted shading indicates the regression is significant at the 90% confidence level.

3.3 Modeling evidence for the physical process of CSA SM -TCEP connection

Although observational analyses reveal a robust statistical linkage between reduced CSA SM and TCEP SST cooling, such correlations alone cannot establish causality due to the short analysis period and confounding influences from co-occurring climate variability. To examine whether CSA SM anomalies can serve as a precursor to tropical Pacific SST variability, we conduct sensitivity experiments using the ICTPGCM model. By prescribing South America SM deficits (see Methods for experimental design), we isolate the atmospheric responses to land surface anomalies, providing evidence that SM anomalies may modulate downstream SST variability through coupled processes. Figure S19 shows the ensemble-mean precipitation response, revealing a distinct north-south dipole anomaly pattern over South America consistent with observations (Fig.6b): local precipitation reductions in CSA and enhanced precipitation in ESA&TA. Figure 7a-c display the ensemble-mean tropical atmospheric circulation response

Accepted for publication in *Journal of Climate*. DOI 10.1175/JCLI-D-25-0407.1.

fields, computed as sensitivity-control simulation differences. In response to the reduction of SM in South America, central tropical Pacific experiences upper - tropospheric convergence and subsidence, accompanied by low - level tropospheric anticyclonic high - pressure anomalies and surface easterly wind anomalies. These simulated responses in velocity potential, surface pressure, and wind anomalies exhibit remarkable consistency with observations. This demonstrates that reduced CSA SM appears to influence anticyclonic and easterly wind anomalies over the tropical central Pacific via modifications to the tropical zonal circulation.

We further apply LBM to examine steady-state atmospheric responses to idealized diabatic heating and cooling anomalies (See the Methods section for detailed experimental design). This experiment helps verify the impact of reduced South America SM on atmospheric circulation over the tropical Pacific, primarily by modulating north-south dipole precipitation-related heating anomaly patterns as shown in Fig.6b. As illustrated in Figure 7 d-f, the combined response to the imposed diabatic heating dipole produces anomalous subsidence over the CSA region, elevating surface pressure and driving low-level divergence with pronounced southerly wind anomalies. This meridional circulation anomaly promotes low-level convergence—and associated upper-level divergence—over ESA&TA. The resultant upper-level divergence propagates westward, inducing descent and convergence over the tropical central Pacific, which generates a low-level anticyclonic anomaly and easterly surface winds. This complete teleconnection pattern aligns closely with both observational analyses and sensitivity experiment results, providing evidence for the potential validity of the proposed physical mechanism.

Accepted for publication in *Journal of Climate.* DOI 10.1175/JCLI-D-25-0407.1.

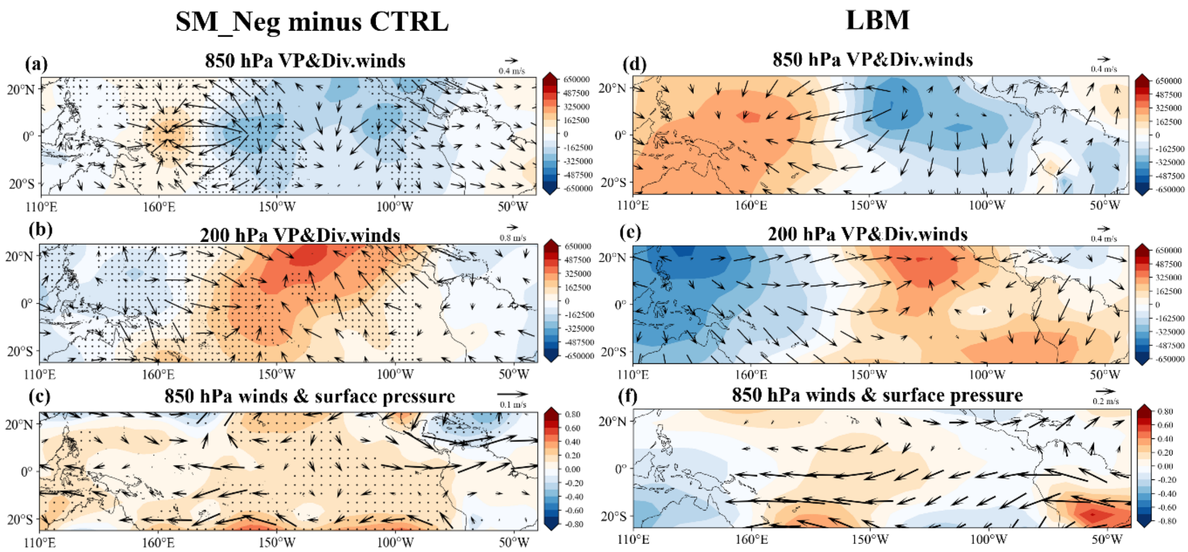

Fig. 7. The results of simulated **(a)** 850 hPa velocity potential (units: m^2/s, shading) and divergent wind (units: m/s, vectors), **(b)** 200 hPa velocity potential (units: m^2/s, shading) and divergent wind (units: m/s, vectors) and **(c)** surface pressure (units: hPa, shading) and 850 hPa wind (units: m/s, vectors) for sensitivity experiments using ICTPGCM model for the spring season response to the reduction of the CSA soil moisture. **(d), (e)** and **(f)** are same as **(a), (b)** and **(c)** respectively, but for the combined LBM responses to diabatic heating over ESA&TA and cooling over CSA. The dotted shading indicates the regions where the results from the sensitivity simulations are significantly different from the control at the 95% confidence level.

To further explore the potential linkage between South American terrestrial drought and tropical circulation changes, we analyze the CESM2 PI-Control simulation—a fully coupled experiment free of anthropogenic forcing. Within this simulation, 30-year sliding trends of the spring CSA SM and winter TCEP SST indices (Fig. 8a) reveal a statistically significant positive correlation ($r = 0.21$, $p < 0.01$). Each pseudo-ensemble member thus represents a 30-year period comparable to the observational record length, with trends arising solely from internal model variability (see Materials and Methods).

To investigate the potential linkage between the pronounced dry CSA SM anomaly and tropical climate changes, we select samples with CSA SM trend absolute values exceeding one standard deviation from the mean of the corresponding time series, minimizing the influence of noise and enhancing the robustness of subsequent statistical analyses. These selected samples are then divided into two distinct groups based on the sign of their SM trends: the positive trend group (characterized by wetting SM) and the negative trend group (exhibiting drying SM).

By comparing the climatological characteristics of the two groups, we examined the associated changes in tropical Pacific SST and atmospheric circulation in response to terrestrial

Accepted for publication in *Journal of Climate.* DOI 10.1175/JCLI-D-25-0407.1.

drought over South America. The composite differences of key meteorological variables between the positive and negative SM trend groups, as depicted in Figures 8b–d, reveal a suite of robust tropical responses that bear a striking resemblance to the observed patterns. Notably, the anomalies exhibit enhanced low-level wind convergence over ESA&TA, consistent with strengthened low-level ascent and an increase in convective precipitation there. The central tropical Pacific displays pronounced low-level divergence, indicative of emergent near-surface anticyclonic anomalies. Concurrently, easterly anomalies intensify across the eastern–central Pacific, accompanied by a well-defined cooling of SSTs in the tropical eastern Pacific. These findings suggest a teleconnection between South American terrestrial drought and tropical Pacific climate variability, supported by the concurrence of tropical SST trends and associated circulation patterns in both observations and CESM2 PI-Control simulations.

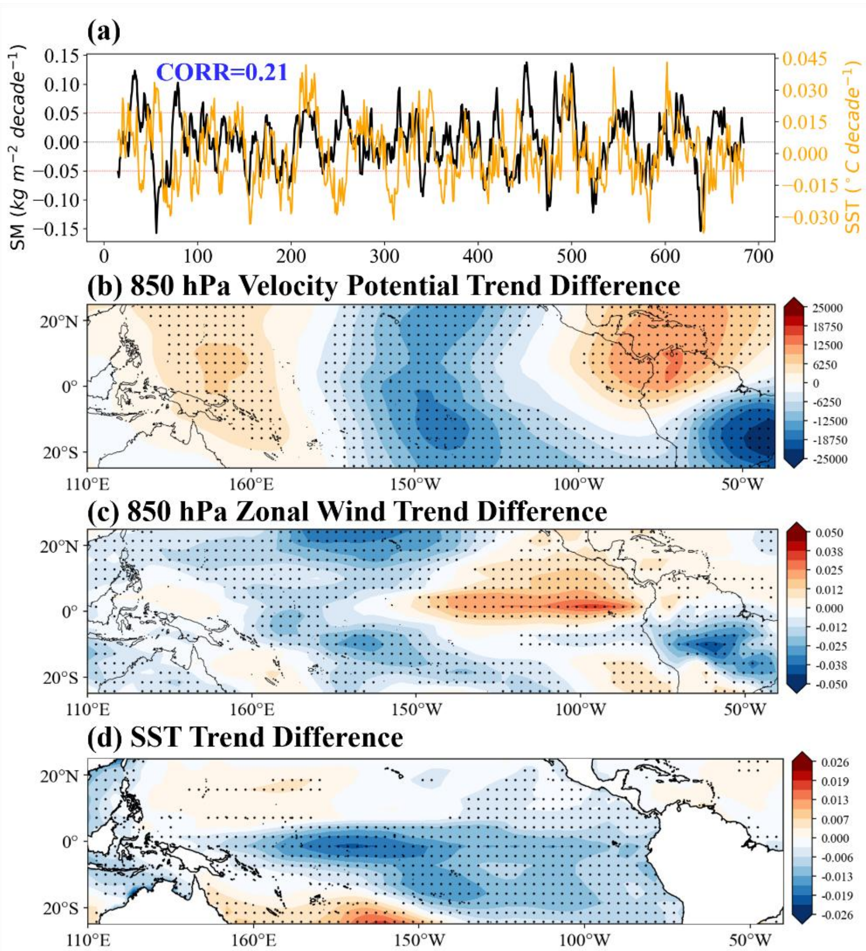

Fig. 8. (a) The linear trend over a 30-year period from CESM2 PI simulation runs within the MAM0 CSA SM and D0JF1 TCEP SST. The differences of **(b)** MAM0 850 hPa velocity potential (unit: m^2/s /decade), **(c)** MAM0 zonal wind (unit: m/s/decade), and **(d)** D0JF1 SST trends (unit: K/decade) between the selected negative and positive cases. The positive and

Accepted for publication in *Journal of Climate*. DOI 10.1175/JCLI-D-25-0407.1.

negative cases satisfy that the absolute values of the CSA SM trend values are greater than one standard deviation (SD) from the mean of the corresponding time series. The dotted areas in **(b)-(d)** denote the significant differences between negative and positive cases based on the two-sample t-test, $p < 0.05$.

4 Conclusions and discussions

Our observational and modeling analyses demonstrate that South America terrestrial drought may serves as a precursor to tropical Pacific SST cooling via a sequence of coupled land–atmosphere–ocean processes. The primary processes are summarized in Figure 9. The reduced CSA SM induces a north-south precipitation dipole across South America, suppressing precipitation over CSA while enhancing precipitation over ESA&TA through land-atmosphere coupling and meridional circulation anomalies. This dipole structure generates enhanced updrafts over ESA&TA that disrupt zonal circulation, inducing divergence and subsidence over the central tropical Pacific. Consequently, low-level anticyclonic high-pressure forms over the central tropical Pacific, generating easterly wind anomalies. These easterlies drive westward warm water transport, equatorial upwelling, and thermocline shoaling across the central-eastern Pacific. Positive Bjerknes feedback then amplifies this cooling, ultimately producing robust cold SST anomalies across the TCEP region.

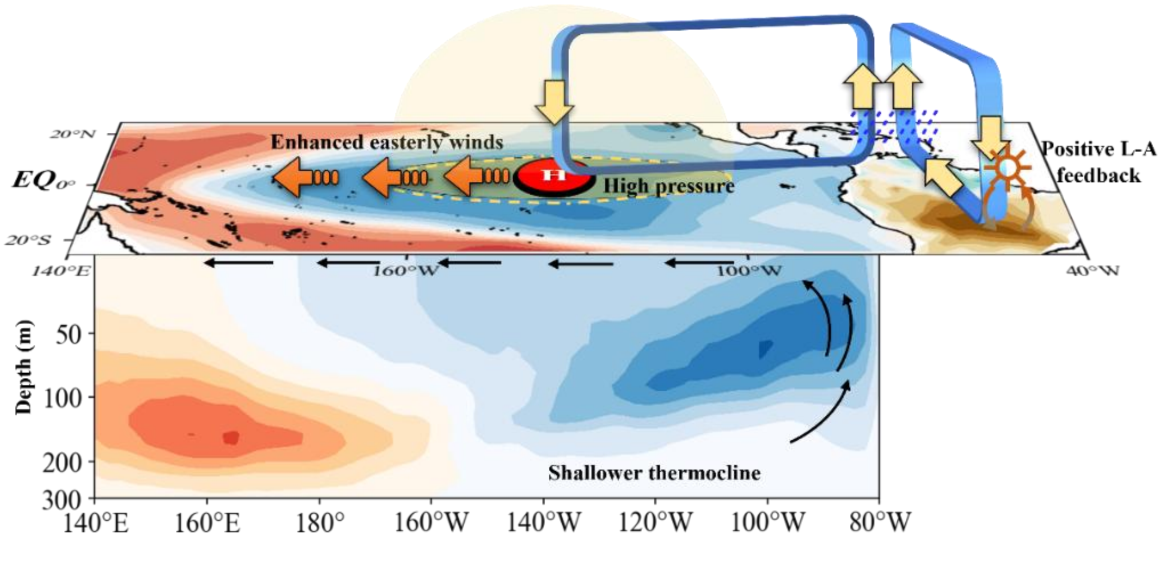

Fig. 9. Schematic summarizing the impact of South America drought on TCEP SST as described in this study. The orange arrows represent surface wind anomalies. The red circle represents high pressure anomalies. The yellow arrow represents the rising and sinking airflow. The brown gradient arrows and the sun symbol represent the feedback processes between soil moisture and atmosphere. Th dots represent positive precipitation anomalies. The blue loops represent the regional Hadley and Walker circulations. The black curved arrows represent the enhanced

Accepted for publication in *Journal of Climate*. DOI 10.1175/JCLI-D-25-0407.1.

upwelling in the eastern equatorial Pacific and the surface westward flow resulting from the stronger easterly winds. See the main text for details of the mechanism.

In this study, our analysis reveals positive SM–precipitation feedbacks in South America, consistent with most studies employing convective parameterization schemes (Hohenegger et al. 2009). However, high-resolution simulations with explicit convection suggest that coarse-resolution models may systematically overestimate the strength of land-atmosphere positive feedbacks, which weaken substantially-or even reverse–in convection-permitting simulations (Yoon and Hohenegger 2025; Lee and Hohenegger 2024). While coarse-resolution models enable robust multi-member ensemble simulations over extended periods to isolate large-scale circulation signals, future high-resolution convection-permitting experiments are essential to test the robustness of these feedbacks and their tele-connected influences.

Existing research emphasizes the critical roles and interplay of internal variability and external forcing in tropical Pacific SST projections (Chung et al. 2024). Several mechanisms have been suggested. For example, the warming of the Indian Ocean influences the multidecadal Pacific climate changes via atmospheric teleconnections (Luo et al. 2012). The ocean initialization in the North Atlantic appears to play a significant role in the predictability of tropical Pacific decadal climate change during the late 1990s(Chikamoto et al. 2012). The recovery of the Antarctic ozone layer and the reduction of aerosol emissions are expected to contribute to a warming trend in the tropical Pacific Ocean(Banerjee et al. 2020). Notably, recent studies have highlighted the importance of land-sea thermal contrast and terrestrial thermal forcing, demonstrating that anomalous heating over tropical and South America land can remotely induce cooling across the eastern and equatorial Pacific via atmospheric teleconnections (Günther et al. 2026). While all these mechanisms need further examination to assess their relative relevance, in future research, we will focus on the role of land-atmosphere feedbacks in modulating tropical Pacific SST variability, aiming to advance the seasonal-to-decadal predictability of tropical Pacific climate.

Acknowledgments

Funding: This work is jointly supported by the National Key Research and Development Program of China (2022YFF0801703).

Accepted for publication in *Journal of Climate.* DOI 10.1175/JCLI-D-25-0407.1.

Author contributions: C.S., designed the research. WL, and CS, performed the data analysis, prepared all figures, and led the writing of the manuscript. All the authors discussed the results and commented on the paper.

Competing interests: The authors declare that they have no competing interests.

Data and materials availability: The original observational data are publicly available. All data sources are mentioned in the Materials and Methods section. The source codes for the analysis of this study are available from the corresponding author upon reasonable request.

Accepted for publication in *Journal of Climate.* DOI 10.1175/JCLI-D-25-0407.1.

Appendix:

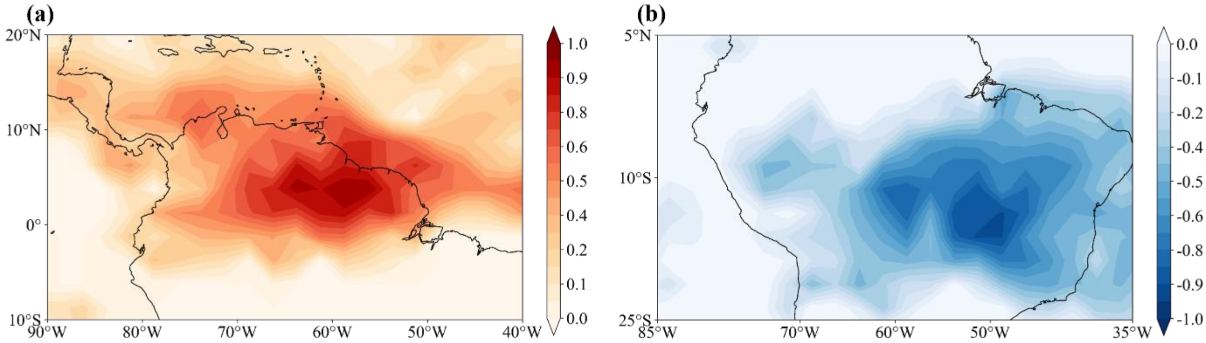

Fig. A1. (a) Idealized heating pattern (applied within 0° – 10° N, 68° W – 50° W) based on the distribution of enhanced precipitation anomalies in ESA&TA region. (b) Idealized cooling pattern (applied within 20° S – 10° S, 65° W – 45° W) based on the distribution of suppressed precipitation anomalies in the CSA region.

Accepted for publication in *Journal of Climate*. DOI 10.1175/JCLI-D-25-0407.1.

Reference

Abatzoglou, J. T., S. Z. Dobrowski, S. A. Parks, and K. C. Hegewisch, 2018: TerraClimate, a high-resolution global dataset of monthly climate and climatic water balance from 1958–2015. *Scientific Data*, **5,** 170191,10.1038/sdata.2017.191.

Amaya, D. J., Y. Kosaka, W. Zhou, Y. Zhang, S.-P. Xie, and A. J. Miller, 2019: The North Pacific Pacemaker Effect on Historical ENSO and Its Mechanisms. *Journal of Climate*, **32,** 7643-7661,https://doi.org/10.1175/JCLI-D-19-0040.1.

Austin, P. C., and J. V. Tu, 2004: Bootstrap Methods for Developing Predictive Models. *The American Statistician*, **58,** 131-137,10.1198/0003130043277.

Banerjee, A., J. C. Fyfe, L. M. Polvani, D. Waugh, and K.-L. Chang, 2020: A pause in Southern Hemisphere circulation trends due to the Montreal Protocol. *Nature*, **579,** 544-548,10.1038/s41586-020-2120-4.

Bjerknes, J., 1969: ATMOSPHERIC TELECONNECTIONS FROM THE EQUATORIAL PACIFIC. *Monthly Weather Review*, **97,** 163-172,https://doi.org/10.1175/1520-0493(1969)097<0163:ATFTEP>2.3.CO;2.

Bretherton, C. S., C. Smith, and J. M. Wallace, 1992: An Intercomparison of Methods for Finding Coupled Patterns in Climate Data. *Journal of Climate*, **5,** 541-560,https://doi.org/10.1175/1520-0442(1992)005<0541:AIOMFF>2.0.CO;2.

Brito, A. L., and Coauthors, 2023: Impacts of increasing greenhouse gas concentrations and deforestation on extreme rainfall events in the Amazon basin: A multi-model ensemble-based study. *International Journal of Climatology*, **43,** 5512-5535,https://doi.org/10.1002/joc.8158.

Cai, W., and Coauthors, 2020: Climate impacts of the El Niño–Southern Oscillation on South America. *Nature Reviews Earth & Environment*, **1,** 215-231,10.1038/s43017-020-0040-3.

Cao, T.-W., F. Zheng, J.-Y. Yu, X.-H. Fang, and W.-X. Zhong, 2024: The Unique Role of the Intraseasonal Zonal Wind in March Over the Equatorial Western Pacific Contributes to Shaping the Subsequent ENSO Development. *Geophysical Research Letters*, **51,** e2024GL110976,https://doi.org/10.1029/2024GL110976.

Capotondi, A., and B. Qiu, 2023: Decadal Variability of the Pacific Shallow Overturning Circulation and the Role of Local Wind Forcing. *Journal of Climate*, **36,** 1001-

Accepted for publication in *Journal of Climate*. DOI 10.1175/JCLI-D-25-0407.1.

1015,https://doi.org/10.1175/JCLI-D-22-0408.1.

Capotondi, A., P. D. Sardeshmukh, and L. Ricciardulli, 2018: The Nature of the Stochastic Wind Forcing of ENSO. *Journal of Climate*, **31,** 8081-8099,https://doi.org/10.1175/JCLI-D-17-0842.1.

Capotondi, A., and Coauthors, 2023: Mechanisms of tropical Pacific decadal variability. *Nature Reviews Earth & Environment*, **4,** 754-769,10.1038/s43017-023-00486-x.

Chen, C.-C., and F. Dominguez, 2024: The Location of Large-Scale Soil Moisture Anomalies Affects Moisture Transport and Precipitation Over Southeastern South America. *Geophysical Research Letters*, **51,** e2023GL106777,https://doi.org/10.1029/2023GL106777.

Chiang, F., O. Mazdiyasni, and A. AghaKouchak, 2021: Evidence of anthropogenic impacts on global drought frequency, duration, and intensity. *Nature Communications*, **12,** 2754,10.1038/s41467-021-22314-w.

Chikamoto, Y., M. Kimoto, M. Watanabe, M. Ishii, and T. Mochizuki, 2012: Relationship between the Pacific and Atlantic stepwise climate change during the 1990s. *Geophysical Research Letters*, **39**,https://doi.org/10.1029/2012GL053901.

Chung, E.-S., and Coauthors, 2024: Tropical eastern Pacific cooling trend reinforced by human activity. *npj Climate and Atmospheric Science*, **7,** 170,10.1038/s41612-024-00713-2.

Eltahir, E. A. B., and R. L. J. Q. J. o. t. R. M. S. Bras, 2010: Precipitation recycling in the Amazon basin, **120**,https://doi.org/10.1002/qj.49712051806.

England, M. H., and Coauthors, 2014: Recent intensification of wind-driven circulation in the Pacific and the ongoing warming hiatus. *Nature Climate Change*, **4,** 222-227,10.1038/nclimate2106.

Espinoza, J.-C., J. C. Jimenez, J. A. Marengo, J. Schongart, J. Ronchail, W. Lavado-Casimiro, and J. V. M. Ribeiro, 2024: The new record of drought and warmth in the Amazon in 2023 related to regional and global climatic features. *Scientific Reports*, **14,** 8107,10.1038/s41598-024-58782-5.

Feron, S., and Coauthors, 2024: South America is becoming warmer, drier, and more flammable. *Communications Earth & Environment*, **5,** 501,10.1038/s43247-024-01654-7.

Geirinhas, J. L., A. Russo, R. Libonati, P. M. Sousa, D. G. Miralles, and R. M. Trigo, 2021: Recent increasing frequency of compound summer drought and heatwaves in Southeast Brazil.

Accepted for publication in *Journal of Climate*. DOI 10.1175/JCLI-D-25-0407.1.

Environmental Research Letters, **16,** 034036,10.1088/1748-9326/abe0eb.

Geirinhas, J. L., A. C. Russo, R. Libonati, D. G. Miralles, A. M. Ramos, L. Gimeno, and R. M. Trigo, 2023: Combined large-scale tropical and subtropical forcing on the severe 2019–2022 drought in South America. *npj Climate and Atmospheric Science*, **6,** 185,10.1038/s41612-023-00510-3.

Giles, J., C. Menéndez, and R. C. Ruscica, 2022: Nonlocal Impacts of Soil Moisture Variability in South America: Linking Two Land–Atmosphere Coupling Hot Spots. *Journal of Climate*, **36,** 1-47,10.1175/JCLI-D-21-0510.1.

Good, S. A., M. J. Martin, and N. A. Rayner, 2013: EN4: Quality controlled ocean temperature and salinity profiles and monthly objective analyses with uncertainty estimates. *Journal of Geophysical Research: Oceans*, **118,** 6704-6716,https://doi.org/10.1002/2013JC009067.

Gore, M., B. J. Abiodun, and F. Kucharski, 2020: Understanding the influence of ENSO patterns on drought over southern Africa using SPEEDY. *Climate Dynamics*, **54,** 307-327,10.1007/s00382-019-05002-w.

Günther, M., S. M. Kang, and Y. Kaspi, 2026: Heating the land cools the eastern and equatorial Pacific, **12,** eaeb7004,doi:10.1126/sciadv.aeb7004.

Ham, Y.-G., J.-S. Kug, J.-Y. Park, and F.-F. Jin, 2013: Sea surface temperature in the north tropical Atlantic as a trigger for El Niño/Southern Oscillation events. *Nature Geoscience*, **6,** 112-116,10.1038/ngeo1686.

Hersbach, H., and Coauthors, 2020: The ERA5 global reanalysis. *Quarterly Journal of the Royal Meteorological Society*, **146,** 1999-2049,https://doi.org/10.1002/qj.3803.

Huang, B., and Coauthors, 2017: Extended Reconstructed Sea Surface Temperature, Version 5 (ERSSTv5): Upgrades, Validations, and Intercomparisons. *J. Clim.*, **30,** 8179-8205,https://doi.org/10.1175/JCLI-D-16-0836.1.

Huang, J., X. Wang, Z. Song, and S. Chen, 2025: Effect of Northeast Pacific Wind on the Improvement of El Niño Prediction in a Climate Model. *Journal of Climate*, **38,** 531-544,https://doi.org/10.1175/JCLI-D-24-0178.1.

Ishii, M., A. Shouji, S. Sugimoto, and T. Matsumoto, 2005: Objective analyses of sea-surface temperature and marine meteorological variables for the 20th century using ICOADS and the Kobe Collection. *International Journal of Climatology*, **25,** 865-

Accepted for publication in *Journal of Climate*. DOI 10.1175/JCLI-D-25-0407.1.

879,https://doi.org/10.1002/joc.1169.

Jiang, Y., and G. Wang, 2024: Soil Moisture Dominates the Land Surface Feedback in the Development of Compound Drought–Heat Extremes in Tropical South America. *Journal of Hydrometeorology*, **25,** 1649-1664,https://doi.org/10.1175/JHM-D-24-0005.1.

Kaplan, A., M. A. Cane, Y. Kushnir, A. C. Clement, M. B. Blumenthal, and B. Rajagopalan, 1998: Analyses of global sea surface temperature 1856–1991. *Journal of Geophysical Research: Oceans*, **103,** 18567-18589,https://doi.org/10.1029/97JC01736.

Kohyama, T., D. L. Hartmann, and D. S. Battisti, 2017: La Niña–like Mean-State Response to Global Warming and Potential Oceanic Roles. *Journal of Climate*, **30,** 4207-4225,https://doi.org/10.1175/JCLI-D-16-0441.1.

Kosaka, Y., and S.-P. Xie, 2013: Recent global-warming hiatus tied to equatorial Pacific surface cooling. *Nature*, **501,** 403-407,10.1038/nature12534.

Kucharski, F., F. Molteni, and J. H. Yoo, 2006: SST forcing of decadal Indian Monsoon rainfall variability. *Geophysical Research Letters*, **33**,https://doi.org/10.1029/2005GL025371.

Kucharski, F., N. Zeng, and E. Kalnay, 2013a: A further assessment of vegetation feedback on decadal Sahel rainfall variability. *Climate Dynamics*, **40,** 1453-1466,10.1007/s00382-012-1397-x.

Kucharski, F., F. Molteni, M. P. King, R. Farneti, I.-S. Kang, and L. Feudale, 2013b: On the Need of Intermediate Complexity General Circulation Models: A "SPEEDY" Example. *Bulletin of the American Meteorological Society*, **94,** 25-30,https://doi.org/10.1175/BAMS-D-11-00238.1.

Latif, M., and Coauthors, 2023: Strengthening atmospheric circulation and trade winds slowed tropical Pacific surface warming. *Communications Earth & Environment*, **4,** 249,10.1038/s43247-023-00912-4.

Lee, T.-H., J.-Y. Yu, Y.-F. Lin, M.-H. Lo, and H.-M. Xiao, 2023: The Potential Influence of Maritime Continent Deforestation on El Niño-Southern Oscillation: Insights From Idealized Modeling Experiments. *Geophysical Research Letters*, **50,** e2023GL105012,https://doi.org/10.1029/2023GL105012.

Li, J., C. Sun, and F.-F. Jin, 2013: NAO implicated as a predictor of Northern Hemisphere mean temperature multidecadal variability. *Geophysical Research Letters*, **40,** 5497-

Accepted for publication in *Journal of Climate*. DOI 10.1175/JCLI-D-25-0407.1.

5502,https://doi.org/10.1002/2013GL057877.

Li, X., Z.-Z. Hu, M. J. McPhaden, C. Zhu, and Y. Liu, 2023: Triple-Dip La Niñas in 1998–2001 and 2020–2023: Impact of Mean State Changes. *Journal of Geophysical Research: Atmospheres*, **128,** e2023JD038843,https://doi.org/10.1029/2023JD038843.

Liu, S., and J. Sun, 2023: Enhanced Influence of Tropical Pacific Sea Surface Temperature Anomalies on Spring Extreme Heat Events Over Mid-High Latitude Eurasia. *Journal of Geophysical Research: Atmospheres*, **128,** e2022JD037837,https://doi.org/10.1029/2022JD037837.

Lou, W., C. Sun, and Y. Liu, 2023: Cross-seasonal influence of the North Tropical Atlantic SST on soil moisture in Northeastern Eurasia. *Climate Dynamics*, **61,** 5845-5860,10.1007/s00382-023-06887-4.

Lou, W., C. Sun, and B. Zuo, 2024a: Concurrent trend turnings of drought severity across Afro-Eurasian continent since 1950. *Global and Planetary Change*, **243,** 104628,https://doi.org/10.1016/j.gloplacha.2024.104628.

Lou, W., C. Sun, F. Kucharski, J. Li, and Y. Liu, 2024b: Amazon drought amplifies SST warming in the North Tropical Atlantic. *Climate Dynamics*, **62,** 9377-9390,10.1007/s00382-024-07400-1.

Lou, W., and Coauthors, 2026: Divergent Mechanisms Drive Multi-Decadal Drought Intensification in South America: A Trend Turning Analysis From 1958 to 2023. *International Journal of Climatology*, **46,** e70242,https://doi.org/10.1002/joc.70242.

Luo, J.-J., W. Sasaki, and Y. Masumoto, 2012: Indian Ocean warming modulates Pacific climate change. *Proceedings of the National Academy of Sciences*, **109,** 18701-18706,10.1073/pnas.1210239109.

McGregor, S., A. Timmermann, M. F. Stuecker, M. H. England, M. Merrifield, F.-F. Jin, and Y. Chikamoto, 2014: Recent Walker circulation strengthening and Pacific cooling amplified by Atlantic warming. *Nature Climate Change*, **4,** 888-892,10.1038/nclimate2330.

McPhaden, M. J., S. E. Zebiak, and M. H. Glantz, 2006: ENSO as an Integrating Concept in Earth Science. *Science*, **314,** 1740-1745,10.1126/science.1132588.

McPhaden, M. J., T. Lee, and D. McClurg, 2011: El Niño and its relationship to changing background conditions in the tropical Pacific Ocean. *Geophysical Research Letters*,

Accepted for publication in *Journal of Climate*. DOI 10.1175/JCLI-D-25-0407.1.

38,https://doi.org/10.1029/2011GL048275.

Molteni, F., F. Kucharski, and R. Farneti, 2024: Multi-decadal pacemaker simulations with an intermediate-complexity climate model. *Weather Clim. Dynam.*, **5,** 293-322,10.5194/wcd-5-293-2024.

Mondal, S. K., S.-I. An, S.-K. Min, T. Jiang, and B. Su, 2024: Enhanced soil moisture–temperature coupling could exacerbate drought under net-negative emissions. *npj Climate and Atmospheric Science*, **7,** 265,10.1038/s41612-024-00820-0.

Muñoz-Sabater, J., and Coauthors, 2021: ERA5-Land: a state-of-the-art global reanalysis dataset for land applications. *Earth Syst. Sci. Data*, **13,** 4349-4383,10.5194/essd-13-4349-2021.

Poveda, G., and O. J. Mesa, 1997: Feedbacks between Hydrological Processes in Tropical South America and Large-Scale Ocean–Atmospheric Phenomena. *Journal of Climate*, **10,** 2690-2702,https://doi.org/10.1175/1520-0442(1997)010<2690:FBHPIT>2.0.CO;2.

Rayner, N. A., and Coauthors, 2003: Global analyses of sea surface temperature, sea ice, and night marine air temperature since the late nineteenth century. *Journal of Geophysical Research: Atmospheres*, **108**,https://doi.org/10.1029/2002JD002670.

Schumacher, V., F. Justino, N. F. Leonardo, and M. P. Pereira, 2022: Disentangling the role of the Pacific and Atlantic Oceans during the Amazonian droughts in 2015. *Theoretical and Applied Climatology*, **148,** 1057-1067,10.1007/s00704-022-03998-6.

Sen, P. K., 1968: Estimates of the Regression Coefficient Based on Kendall's Tau. *Journal of the American Statistical Association*, **63,** 1379-1389,10.2307/2285891.

Seneviratne, S., R. Koster, Z. Guo, and P. Dirmeyer, 2004: Soil moisture memory in AGCM simulations: Analysis of Global Land-Atmosphere Coupling Experiment (GLACE) Data. *AGU Spring Meeting Abstracts*, 05

Seneviratne, S. I., and Coauthors, 2010: Investigating soil moisture–climate interactions in a changing climate: A review. *Earth-Science Reviews*, **99,** 125-161,https://doi.org/10.1016/j.earscirev.2010.02.004.

Spennemann, P. C., and A. C. Saulo, 2015: An estimation of the land-atmosphere coupling strength in South America using the Global Land Data Assimilation System. *International Journal of Climatology*, **35,** 4151-4166,https://doi.org/10.1002/joc.4274.

Staal, A., B. M. Flores, A. P. D. Aguiar, J. H. C. Bosmans, I. Fetzer, and O. A. Tuinenburg, 2020:

Accepted for publication in *Journal of Climate*. DOI 10.1175/JCLI-D-25-0407.1.

Feedback between drought and deforestation in the Amazon. *Environmental Research Letters*, **15,** 044024,10.1088/1748-9326/ab738e.

Vimont, D. J., J. M. Wallace, and D. S. Battisti, 2003: The Seasonal Footprinting Mechanism in the Pacific: Implications for ENSO. *Journal of Climate*, **16,** 2668-2675,https://doi.org/10.1175/1520-0442(2003)016<2668:TSFMIT>2.0.CO;2.

Wang, B., and Coauthors, 2023: Understanding the recent increase in multiyear La Niñas. *Nature Climate Change*, **13,** 1075-1081,10.1038/s41558-023-01801-6.

Wang, C., and P. C. Fiedler, 2006: ENSO variability and the eastern tropical Pacific: A review. *Progress in Oceanography*, **69,** 239-266,https://doi.org/10.1016/j.pocean.2006.03.004.

Watanabe, M., and F.-F. Jin, 2003: A Moist Linear Baroclinic Model: Coupled Dynamical–Convective Response to El Niño. *J. Clim.*, **16,** 1121-1139,https://doi.org/10.1175/1520-0442(2003)16<1121:AMLBMC>2.0.CO;2.

Wei, S., X. Wang, C. Wang, and Q. Xie, 2024: El Niño phase transition by deforestation in the Maritime Continent. *npj Climate and Atmospheric Science*, **7,** 3,10.1038/s41612-023-00548-3.

Xie, P., and P. A. Arkin, 1997: Global Precipitation: A 17-Year Monthly Analysis Based on Gauge Observations, Satellite Estimates, and Numerical Model Outputs. *Bulletin of the American Meteorological Society*, **78,** 2539-2558,https://doi.org/10.1175/1520-0477(1997)078<2539:GPAYMA>2.0.CO;2.

Xu, X., X. Zhang, W. J. Riley, Y. Xue, C. A. Nobre, T. E. Lovejoy, and G. Jia, 2022: Deforestation triggering irreversible transition in Amazon hydrological cycle. *Environmental Research Letters*, **17,** 034037,10.1088/1748-9326/ac4c1d.

Zalles, V., and Coauthors, 2021: Rapid expansion of human impact on natural land in South America since 1985. *Science Advances*, **7,** eabg1620,10.1126/sciadv.abg1620.

Zeng, N., J.-H. Yoon, J. A. Marengo, A. Subramaniam, C. A. Nobre, A. Mariotti, and J. D. Neelin, 2008: Causes and impacts of the 2005 Amazon drought. *Environmental Research Letters*, **3,** 014002,10.1088/1748-9326/3/1/014002.

Zuo, B., Z. Hou, F. Zheng, L. Sheng, Y. Gao, and J. Li, 2020: Robustness Assessment of the RSD t-Test for Detecting Trend Turning in a Time Series. *Earth and Space Science*, **7,** e2019EA001042,https://doi.org/10.1029/2019EA001042.

Accepted for publication in *Journal of Climate*. DOI 10.1175/JCLI-D-25-0407.1.